Proceedings World Geothermal Congress 2020+1
Reykjavik, Iceland, April - October 2021

Evaluation of the Efficiency of an Organic Corrosion Inhibitor in the Upper Rhine Graben Under Geothermal Conditions

Linda Makni[1], Petra Huttenloch[1], Roman Zorn[1], Hagen Steger[2], Wolfgang Hater[3], Philipp Blum[2]

[1] European Institute for Energy Research, Emmy-Noether-Str. 11, 76131 Karlsruhe

[2] Karlsruhe Institute for Technology, Kaiserstr. 12, 76131 Karlsruhe

[3] Kurita Europe GmbH, Giulinistr. 2, 67065 Ludwigshafen

makni@eifer.org

Keywords: CO_2 corrosion, inhibitor performance, NaCl- and Na-Ca-Cl-brine, carbon steel, geothermal environment, electrochemical studies, weight loss tests

ABSTRACT

The Upper Rhine Graben in Central Europe has a significant thermal anomaly, which makes it a promising candidate for the geothermal exploitation. However, the high saline, CO_2-enriched geothermal brines can potentially cause corrosion leading to material failure and expensive downtimes of geothermal power plants. One possibility to prevent corrosion is the addition of chemical inhibitors into the circulating geothermal fluids. In this contribution, the inhibitor efficiency of an imidazoline based corrosion inhibitor is evaluated. Apart from testing of an original geothermal brine sampled at a geothermal power plant at the western part of the Upper Rhine Graben artificial brines with different Na-Ca-Cl contents are examined. To assess the inhibition effect of the tested inhibitor, selected electrochemical (potentiodynamic polarization, impedance spectroscopy) and weight loss tests are applied. Thereby, the corrosion behavior of a common mild steel is examined which is a typical example for the materials used in geothermal power plants. Experiments are performed at 80°C under CO_2 conditions. As one major outcome of the study, the inhibition effect of the examined inhibitor turned out to be largely dependent on the interplay of the chemically active species in the brine and the inhibitor itself. Based on the experimental results, a conceptual model of the adsorption/desorption behavior of the inhibitor and its mutual interaction with the studied brines is developed.

1. INTRODUCTION

During the last decades, several geothermal power plants have been installed in the Upper Rhine Graben (URG) (Sanjuan et al. 2016). The region located in Central Europe is particularly interesting for the exploitation of geothermal heat because of the elevated heat flow of up to 120 W/m² and the high underground temperatures found at shallow depth (e.g. 120°C in 800 m depth in Soultz-sous-Forêts, France) (Pribnow and Schellschmidt 2000). However, this advantage of the URG is mitigated by the high salinary geothermal brines (<200 g/l) circulating in the geothermal power plants (Sanjuan et al. 2016). Due to temperature and pressure gradients, the low average pH values (< 5), the high chloride content (≥ 60 g/l) and variations of the flow velocity, different chemical compounds of the brines can be precipitated and corrosion processes can deteriorate the steel parts of the power plant. In the long term, these circumstances lead to premature material failure and thus high maintenance costs (Finsgar and Jackson 2014).

The corrosion process can be explained as an electrochemical process with an anodic and a cathodic reaction, taking place at the interface between the geothermal brine and the steel. The iron in the steel oxidizes in contact with the brine by releasing two electrons (anodic reaction). These electrons interfere with hydrogen ions present in the acidic brine (cathodic reaction). CO_2 bearing brines could trigger the cathodic reaction by forming H_2CO_3:

$$Fe \rightarrow Fe^{2+} + 2e^- \quad (1)$$

$$2H^+ + 2e^- \rightarrow H_2 \quad (2)$$

$$2H_2CO_3 + 2e^- \rightarrow H_2 + 2HCO_3^- \quad (3)$$

$$2HCO_3^- + 2e^- \rightarrow H_2 + 2CO_3^{2-} \quad (4)$$

On the other hand, dissolved Fe^{2+} can react with CO and form siderite ($FeCO_3$). The latter can precipitate on the steel surface and form protective layers, which slow down the corrosion process (Heuer and Stubbins 1999, Mundhenk et al. 2013).

One possibility to face corrosion and/or scaling is the use of chemical inhibitors. Inhibitors have already been successfully used in the petroleum industry (Jovancicevic et al.1999). During the last years, they were partly used at different geothermal sites. However, their reaction behavior is not yet fully understood and the optimal working conditions of corrosion inhibitors in geothermal applications are mostly unknown. For this reason, this study aims to examine the performance of one promising corrosion inhibitor at the example of the URG geothermal environment. Therefore, mild steel samples are exposed to both original brine sampled at the Soultz-sous-Forêts power plant (France) and to artificial brines set up to resemble the original geothermal conditions in the URG. By applying different electrochemical measurement techniques, key performance parameters of the inhibitor such as the inhibitor efficiency and corrosion rate are determined and systematically compared at different operating conditions. With these results, the behavioral model of the inhibition effect of the inhibitor is proposed.

2. MATERIALS AND METHODS

2.1 Geothermal Brines: Chemical Composition

The corrosion studies are carried out with four different brines: 1) pure NaCl solution, 2) Na-Ca-Cl solution 3) artificial geothermal brine (Table 1) and 4) original brine (Table 2) sampled at the production well of the geothermal power plant in Soultz-sous-Forêts. All artificial brines were prepared from analytical grade chemicals. The high mineralization was adjusted to the chemical composition of the produced brine at the Soultz-sous-Forêts geothermal site. Further information on the chemical composition of the original brine is given in Scheiber et al. (2015). Variation of the chemistry of the original brine caused by degassing, cooling down and precipitations cannot be avoided. If not else stated the brines are deaerated at least for 30 minutes with a vacuum pump and purged with CO_2 (4.8 technical grade) in a special designed pressure chamber for at least 20 minutes.

Table 1: Chemical composition of the tested brines.

	NaCl (g/L)	$CaCl_2$ (g/L)	KCl (g/L)	$SrCl_2$ (g/L)	Na_2SO_4 (g/L)
NaCl brine	98.91	-	-	-	-
Na-Ca-Cl brine	78.49	19.38	-	-	-
Artificial brine	77.00	19.00	6.50	1.18	0.39

	Total Cl-content (g/L)	Total Ca-content (g/L)
NaCl brine	60	0
Na-Ca-Cl brine	60	7.0
Artificial brine	62	6.9
Original brine	56	7.6

Table 2: Chemical composition of the original brine at the production site according to Scheiber et al. (2015) with *c* = concentration (g/L).

	c (g/L)		*c* (g/L)
Na	25.80	Cs	0.02
Ca	7.60	Rb	0.03
K	3.74	As_{total}	0.01
Sr	0.41	Cl	56.00
Li	0.19	Br	0.23
Mg	0.14	SO_4	0.15
Ba	0.03	HCO_3	0.16
NH_4	0.02	F	0.01
Fe_{total}	0.04	B	0.04
Mn	0.02	SiO_2	0.20

2.2 Carbon Steel

A common carbon steel (C45+C) is used in all corrosion experiments. The chemical composition of the steel is given in Table 3. The steel coupons have a diameter of around 3 cm, a thickness of around 0.3 cm and a mass density of 7.85 g/cm³. Before each experiment, the steel coupons are ground according to ASTM-G5-82 with SiC abrasive paper with three different granularities (180, 320 and 1000), cleaned with distilled water, degreased in acetone and dried.

Table 3: Chemical composition of the tested carbon steel in weight percent (wt-%).

	C	Si	Mn	P	S	Cr	Mo	Ni	Fe
C45+C (1.0503)	0.42 – 0.5	<0.4	0.5 – 0.8	<0.045	<0.045	<0.4	<0.1	<0.4	Bal.

2.3 Inhibitor

A hydroxyethyl-imidazoline-based, organic corrosion inhibitor (provided by KURITA Company, Germany) is used. The detailed chemical composition underlies intellectual property restrictions and is therefore not known to the authors. Generally, the chemical agent imidazoline consists of a five membered ring with two nitrogen atoms and three carbon atoms. One nitrogen atom is connected to the neighboring carbon by a double bounding. A hydrophobic alkyl chain is attached to the carbon, which prevents water molecules from adsorbing onto the metal surface. A hydrophilic functional group is attached to a nitrogen atom, which additionally controls the adsorption behavior of the inhibitor (Jevremovic et al. 2016).

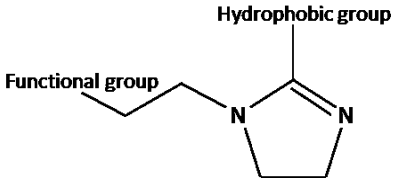

Figure 1: General structure of a hydroxyethyl imidazoline.

2.4 Weight loss tests

Weight loss experiments were performed with steel coupons in the Na-Ca-Cl brine locked in a PTFE vessel (400 ml) at 80°C in the oven. To avoid contact corrosion the steel samples are placed in a Teflon holder. After 24 h (96 h) of exposition, the samples are cleaned with inhibited acid and distilled water according to ASTM G 1-03 (2011), and subsequently weighed. The experiments are conducted under non-stirring conditions.

The corrosion rate C_R (mm/years) is calculated as a function of the steel surface A (cm²), the mass loss Δm (g), exposure time t (years) and steel density ρ (g/cm³):

$$C_R = \frac{\Delta m}{A \cdot t \cdot \rho} \tag{5}$$

The efficiency of the inhibitor IE (%) is determined by weighing the steel samples before and after exposition in the oven:

$$IE = \frac{m_{blank} - m_{inhibitor}}{m_{blank}} \cdot 100 \tag{6}$$

Where m_{blank} is representing the mass loss of the blank steel sample and $m_{inhibitor}$ is the mass loss of the inhibited steel.

2.5 Electrochemical measurements

The electrochemical measurements are conducted with a KMZ 5 AEH corrosion cell system provided by Sensortechnik Meinsberg GmbH. It consists of a three electrode setup with a double-walled glass cell (nominal volume 500 ml) and a voltmeter. The glass cell is tempered by a thermostat F25 (Julabo GmbH). The electrode setup consists of a working electrode, that comprises the sample placed in a sealed plastic housing (exposed sample surface: 0.76 cm²), a counter electrode consisting of a platinum platelet that is positioned face-to-face at a constant distance to the working electrode and a Ag/AgCl reference electrode saturated in a 3M KCl. A Haber-Luggin capillary with a salt bridge connect the reference with the working electrode.

A Teflon-coated stirrer is used to homogenize the electrolyte solution (80 rpm). In this study, all experiments are conducted at ambient pressure and at a temperature of 80°C. This temperature set represents the temperature at the reinjection site of the Soultz-sous-Forêts geothermal power plant. In order to obtain representative results, experiments were performed three times.

2.5.1 Potentiodynamic polarization (PP)

Polarization measurements aim at the characterization of the corrosion response of the system. After one hour of immersion time the open circuit potential (OCP) is measured and the potentiodynamic polarization measurement is started. Therefore, a potentio-dynamic scan in the potential range of ± 250 mV versus the previously determined OCP value is applied. In the scan the potential is set to the maximum negative value first (-250 mV versus OCP, cathodic polarization) and then increased with a slew rate of 0.16 mV/s towards the anodic branch. The scan is interrupted if the measured current exceeds the critical value j_{crit} = 100 µA. The sampling rate is set to a fixed value of 0.1 s^{-1}. The measurement parameters are chosen according to ASTM G5-82 standard. The software "LMRemote 2000" provided by Sensortechnik Meinsberg GmbH is used to control the potential, to record the polarization curves and to construct the Tafel slopes β_a and β_c manually. The polarization resistance R_p is determined by the linear regression of the non-logarithmic polarization curve close to E_{corr}. With the Stern-Geary equation, the Tafel-slopes can be obtained by (Moreland and Rowlands, 1977):

$$j_{corr} = \frac{\beta_a \beta_c}{2{,}303 \cdot (\beta_a + \beta_c)} \cdot \frac{1}{R_p} = \frac{B}{R_p} \tag{7}$$

Where j_{corr} is the corrosion current density (µA/cm²), β_a and β_c are the anodic and cathodic Tafel slopes (V/dec) and R_p is the polarization resistance (Ωm²)

The corrosion rate is be determined as (ASTM G102-89, 2010):

$$C_R = 0.00327 \cdot \frac{j_{corr} \cdot EW}{\rho} \quad (8)$$

Where 0.00327 is a conversion factor (mm/y), j_{corr} is the corrosion current density (µA/cm²), EW is the equivalent weight of the corroding species (g), ρ is the steel density (g/cm³)

The inhibitor efficiency is calculated as:

$$IE = \frac{j_{corr}(blank) - j_{corr}(inhibitor)}{j_{corr}(blank)} \cdot 100 \quad (9)$$

Where j_{corr}(blank) is representing the corrosion current density without the inhibitor whereas j_{corr}(inhibitor) is representing the corrosion current density of the inhibited sample.

2.5.2 Electrochemical impedance spectroscopy (EIS)

Impedance spectroscopy tests were carried out with an electrochemical workstation of Zahner-Elektrik GmbH. EIS measurements were conducted at open-circuit potential, with a perturbation amplitude of 10 mV and in the frequency range 100 kHz -15 mHz. To analyze the obtained impedance spectra a set of equivalent circuits were evaluated and fitted to the measured impedance. Further details about the experimental setup and the fitting procedure can be found in Huttenloch, P. et al. (2019).

The inhibitor efficiency was calculated from the charge transfer resistance obtained from the model fit as follows (Huttenloch et al., 2019):

$$IE = \frac{1/R_{ct}(blank) - 1/R_{ct}(inhibitor)}{1/R_{ct}(blank)} \cdot 100 \quad (10)$$

Thereby R_{ct}(blank) and R_{ct}(inhibitor) correspond to the charge transfer resistance of the pristine and inhibited system, respectively.

3. RESULTS AND DISCUSSION

3.1 Weight loss tests

Steel samples have been exposed to a Na-Ca-Cl brine during 24 h and 96 h at 80°C. In Table 1Table 4 the results of the mass loss are listed. Apparently, the corrosion rate of the uninhibited brine after 24 h (C_R = 0.67 mm/a) of exposition is significantly higher than after 96 h (C_R = 0.24 mm/a). This observation points towards the formation of carbonate scales like $FeCO_3$ or $CaCO_3$ that gradually precipitate on the metal surface as a function of time. The layer gets thicker over time and therefore the dissolution of iron is slowed down (Liu et al., 2001 and Wu et al., 2014). In the inhibited brine, the corrosion rate decreased after the addition of 100 ppm and 200 ppm of the inhibitor by around 50%. Inhibitor concentrations larger than 200 ppm did not further increase the inhibitor efficiency. Presumably, the stagnant conditions in the weight loss tests induce the efficiency saturation at certain inhibitor concentrations as a constant coverage of the steel surface with inhibitor species is reached. Further research at non-steady conditions (e.g. by stirring the solution during the weight loss tests) is needed to validate this assumption.

It is remarkable that the corrosion rate increases with a longer exposition time of 96 h from 0.24 mm/a in the uninhibited brine to 0.38 mm/a in the inhibited brine. This behavior can be explained in two different ways: Either the inhibitor competes with the protective carbonate scales meaning that the carbonate molecules are attached on the metal surface blocking free metal surface for the inhibitor molecules. The second explanation aims at the available amount of the inhibitor. As iron particles are released from the metal surface, these particles could attract the inhibitor and therefore reduce the inhibitor concentration at the metal surface. In both cases, this finding points out that a continuous dosage of the inhibitor might be useful to reduce corrosion.

Figure 2 a-c illustrates the steel coupons before and after weight loss tests. Figure 2b displays the uninhibited sample after exposition in the Na-Ca-Cl brine. A thin layer of non-soluble corrosion products covers the entire metal surface. In contrast, the metal surface was only partly covered with corrosion products in the inhibited sample (Figure 2c). This indicates that the inhibitor is at least partly adsorbed at the metal surface and inhibited the onset of corrosion processes.

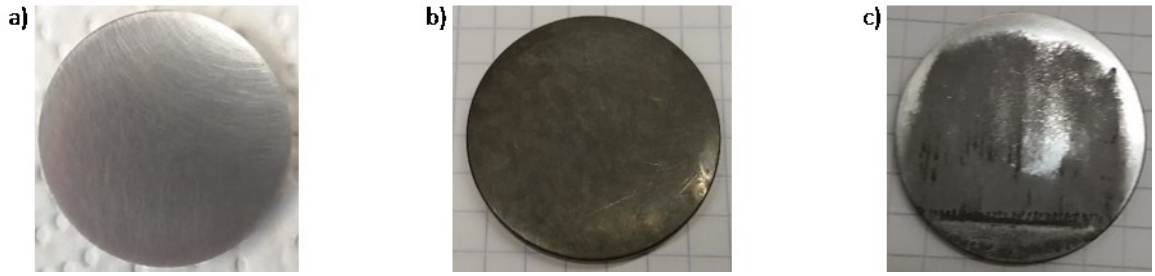

Figure 2: Steel samples before and after exposition in Na-Ca-Cl brine. a) Sample before exposition. b) Sample after exposition without inhibitor. c) Sample after exposition with inhibitor.

Table 4: Data obtained from weight loss tests as a function of the exposition time and inhibitor concentration *c* at 80°C.

t (h)	*c* (ppm)	*A* (cm²)	*Δm* (g)	C_R (mm/a)	*IE* (%)
24	0	19.09	0.028	0.67	-
24	100	18.88	0.014	0.35	49
24	200	19.05	0.012	0.30	56
24	500	19.04	0.019	0.47	30
96	0	19.14	0.039	0.24	-
96	200	19.07	0.063	0.38	-

3.2 Electrochemical measurements

3.2.1 Potentiodynamic polarization (PP)

The influence of the inhibitor concentration on the corrosion rate is determined in the artificial brine, which is shown in Figure 3 a and Table 5. In the uninhibited brine, the determined E_{corr} value equals -657 mV and j_{corr} calculated according to equation 7 is 51 µA/cm². The addition of the inhibitor reveals a slight shift of the polarization curve to less negative potential values. The E_{corr} is reduced by $\Delta E_{corr} = 45$ mV indicating an anodic inhibitor type suppressing the anodic corrosion reaction. This result is in good accordance with results found in literature where hydroxyethyl-imidazoline is identified as an anodic inhibitor type (Ortega-Toledo et al. 2010). However, according to Tao et al. (2009) a shift of the E_{corr} less than 85 mV is attributed to a mixed type inhibitor that is reducing both the anodic iron dissolution and the cathodic hydrogen evolution reactions. Other authors (Jevremovic et al. 2016, Liu and Zheng 2013) identified imidazoline as a mixed type inhibitor with a slight trend to anodic inhibition. The highest inhibition efficiency is obtained at 100 ppm of the inhibitor concentration. With an $IE = 52\%$ the corrosion rate is reduced from 0.59 mm/a to 0.28 mm/a. Higher dosage of the inhibitor does not enhance the inhibitors efficiency in the tested brine.

The geothermal fluids of the studied environment in the URG are enriched with CO_2 (Sanjuan et al. 2016). Thus, electrochemical corrosion measurements in CO_2 atmosphere are expected to reflect the real world application to a higher extent than the measurements in O_2 atmosphere. Nevertheless, the comparison of both atmospheres is helpful to understand the corrosion behavior in case of leakages in the pipelines or by natural diffusion of oxygen into the system. The polarization scans are conducted at 80°C with inhibited and uninhibited artificial brine. The scans (Figure 3b and Table 5) show major differences in the current density of the cathodic branch. As explained in section 1 CO_2 is reduced to H_2CO_3 leading to formation of additional hydrogen. As the cathodic branch represents the hydrogen formation, the current density increases in comparison to the CO_2 free measurement resulting in significantly higher j_{corr} values (14 µA/cm² vs. 51 µA/cm²). This result has also been observed in other publications e.g. Nesic et al. (1996). Inhibiting the solution leads to a shift of the polarization curves in both cases (CO_2 and O_2) towards more positive E_{corr} values demonstrating the earlier determined anodic character of the inhibitor. The current exchange density is decreased at both conditions but is more pronounced for the CO_2 containing system indicating a better adsorption behavior of the inhibitor in CO_2 environment. In literature imidazoline-based inhibitors have already been successfully used for the prevention of CO_2- corrosion (Heydari and Javidi 2012; Jevremović et al. 2013; Liu et al. 2009). The addition of the inhibitor to the CO_2-containing solution displays the formation of a plateau in a certain potential area of the anodic branch and a sudden increase of the current density. Zhang et al. 2007 explain this increase as a result of the desorption of the inhibitor. Furthermore, the anodic branches of the uninhibited and the inhibited solution intersect at high potential values demonstrating that at this point the inhibitor is completely desorbed from the metal surface. The inhibition efficiencies for both configurations (with and without CO_2) are demonstrating the favorable CO_2 inhibition behavior of the imidazoline with a maximum efficiency of 30 % compared to $IE_{max} = 20$ % ($c_{inhibitor}$=500ppm) in the CO_2-free environment. Nevertheless, the obtained *IE* are generally lower than in literature where *IE* of up to 99.8% are reached (Jevremović et al. 2016).

Mild steel coupons have been exposed in four different geothermal brines to evaluate the efficiency of the inhibitor as a function of the brines chemistry. In case of the uninhibited NaCl, Na-Ca-Cl and the artificial brines addition of Ca^{2+}-ions has a significant impact on the corrosion rate C_R of the steel (Figure 4a). The C_R decreases from 1.56 mm/a in the pure NaCl brine to 0.59 mm/a in the artificial brine and 0.51 mm/a in the Na-Ca-Cl brine, respectively (Table 1). The E_{corr} is shifted towards the anodic direction, indicating the formation of a carbonate film. The cathodic partial reaction is significantly decreased in presence of Ca^{2+}-ions which also supports the assumption of film forming reactions on the metal surface (Hernandez et al., Liu et al., Lopez et al 2003). Generally, the polarization behavior of Na-Ca-Cl brine and artificial brine is almost the same in the uninhibited case. This finding is feasible because the composition of the brines matches with respect to the concentration of the main components (NaCl and $CaCl_2$). On the other hand, the observation supports the assumption that the additional species in the artificial brine (KCl, $SrCl_2$ and Na_2SO_4) have no significant influence on the corrosion behavior.

The highest inhibition efficiency is reached in the NaCl brine. The addition of 100 ppm inhibitor revealed an efficiency of 75% whereas in the Ca^{2+} containing brines the *IE* reaches 50%. The poorer inhibition efficiency may be explained by a competitive behavior between the Ca^{2+} ions and the inhibitor for free adsorption sites on the metal surface resulting in a decrease of the inhibition efficiency. The polarization curves of the inhibited brines show a sudden, steep increase of the current density at a potential of approximately - 500 mV indicating the desorption of the inhibitor from the metal surface.

Comparing the artificial brine with the original brine sampled at the geothermal power plant in Soultz-sous-Forets the measured potentiodynamic curve is slightly different (Figure 4b). The determined C_R of the uninhibited (C_R=0.04 mm/a) and inhibited ($C_R = 0.03$ mm/a) original brine is by a factor of 10 smaller than in the artificial brine ($C_R = 0.59$ mm/a) (Table 5). This result might

be explained by the more complex composition, in particular, the larger concentration of earth alkali metals (Ca, Mg, Ca, Sr) and residual organic components in the original brine favoring the formation of carbonates and organic surface films leading to a passivation of the metal surface. However, these components might compete with the inhibitor molecules resulting in a smaller inhibitor efficiency (*IE* = 20%) compared to the artificial brine (*IE* = 30%).

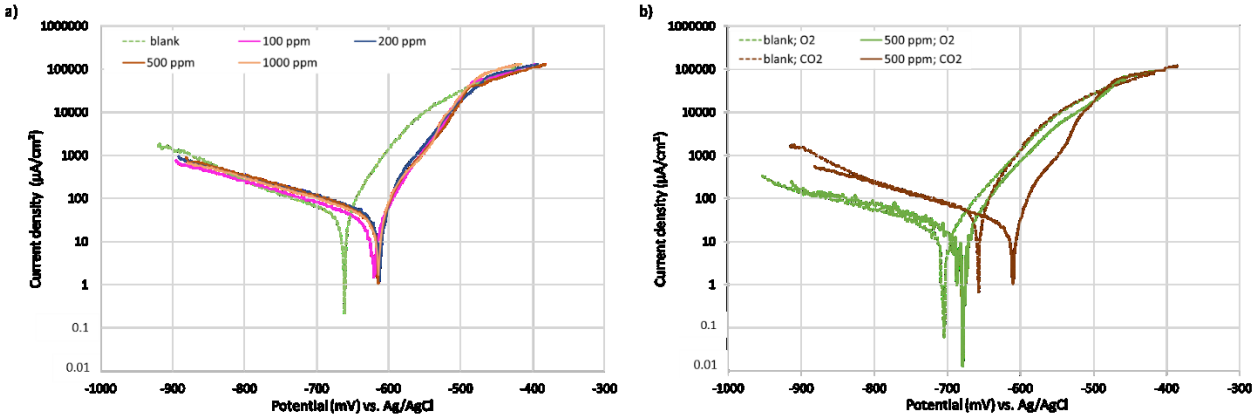

Figure 3: Measured polarization curves (*T* = 80°C, immersion time = 1 h, artificial brine): a) curves as a function of inhibitor concentration. b) Comparison of the inhibition efficiency in O_2 and CO_2 environment.

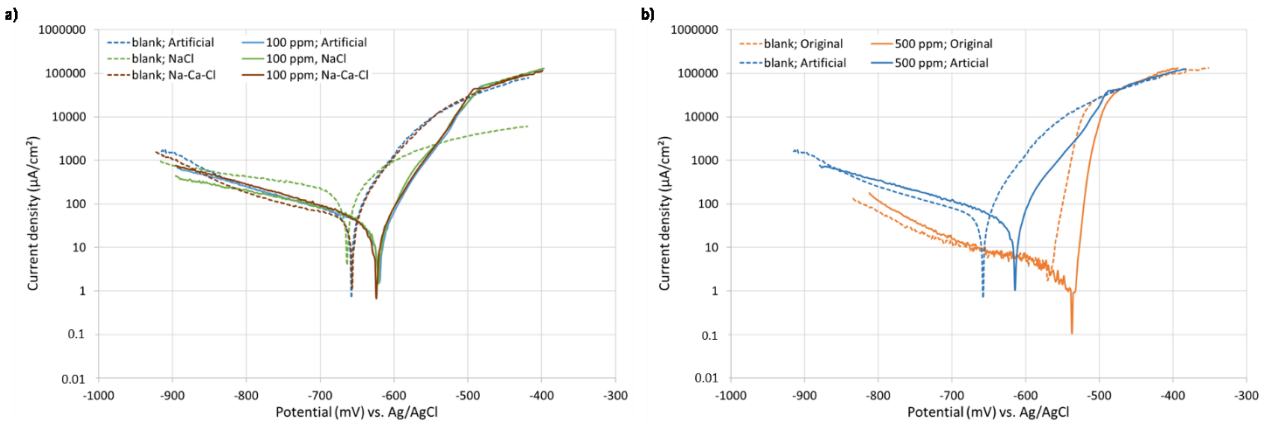

Figure 4: Measured potentiodynamic polarization curves. Determination of the inhibition efficiency in four different geothermal brines (*T* = 80°C Immersion time = 1 h, CO_2 environment): a) Comparison of the artificial brine with NaCl and Na-Ca-Cl brine. b) Comparison of the artificial brine with the original brine. To keep the overview, only one inhibited curve of each brine is displayed here.

Table 5: Electrochemical data obtained from potentiodynamic measurements depending on brine chemistry and inhibitor concentration and surrounding gas with *c* = inhibitor concentration.

Brine	Gas	*c* (ppm)	E_{corr} (mV)	β_c (mV/dec)	β_a (mV/dec)	j_{corr} (µA/cm²)	C_R (mm/a)	*IE* (%)
Artificial	CO_2	0	-657	-166	33	51	0.59	-
Artificial	CO_2	100	-622	-209	45	24	0.28	52
Artificial	CO_2	200	-612	-220	42	30	0.35	41
Artificial	CO_2	500	-618	-229	35	36	0.41	30
Artificial	CO_2	1000	-614	-213	36	35	0.41	30
NaCl	CO_2	0	-668	-374	58	134	1.56	-
NaCl	CO_2	100	-621	-307	46	34	0.40	75
Na-Ca-Cl	CO_2	0	-658	-212	35	44	0.51	-
Na-Ca-Cl	CO_2	100	-621	-209	44	26	0.31	41
Original	CO_2	0	-567	-162	17	4	0.04	-
Original	CO_2	500	-533	-193	8	3	0.03	20
Artificial	O_2	0	-702	-246	58	14	0.16	-
Artificial	O_2	500	-679	-212	53	13	0.15	6

3.2.2 Electrochemical impedance spectroscopy (EIS)

EIS measurements are performed with the Na-Ca-Cl brine at 80°C and different inhibitor concentrations (0-500 ppm). The Nyquist plot (Figure 5c) shows that the impedance response changes with increasing inhibitor concentrations. For the uninhibited brine and experiments up to 50 ppm inhibitor concentration, the Nyquist plot shows a depressed capacitive loop in the middle to low-frequency range and a diffusion phenomenon (Warburg impedance) in the low frequency range. The equivalent circuit in Figure 5a) can best describe this impedance behavior. For inhibitor concentrations ≥100 ppm the Nyquist plot shows only one capacitive loop which is interpreted in terms of the equivalent circuit shown in Figure 5b). With increasing inhibitor concentrations up to 200 ppm, the diameter of the semicircles increases significantly. According to Huttenloch et al. (2019), the capacitive loop can be attributed to the charge transfer process at the steel surface whereas the diffusion feature relates to the transport of electroactive species to the surface. Therefore, it seems meaningful that the diameter of the capacitive loop increases with increasing inhibitor concentration as the passivation layer formed by the inhibitor is more pronounced in this case. This interpretation is supported by the growing R_{ct} values as depicted in Table 6. The depression of the capacitive loop gets apparent in the *n*-value of the considered constant phase element and can be explained by the surface inhomogeneity and heterogeneous adsorption of the inhibitor. The prominence of the diffusion feature decreases significantly with increasing inhibitor concentrations. For a more detailed investigation of the impedance behavior the reader is referred to Huttenloch et al. (2019). The highest inhibitor efficiency is achieved by addition of 200 ppm of the inhibitor which is in good accordance with the results obtained in the weight loss tests. Higher inhibitor concentrations resulted in a decrease of the efficiency. The increase of the inhibitor efficiency up to a critical inhibitor concentration was also observed with the potentiodynamic polarization scans and weight loss tests.

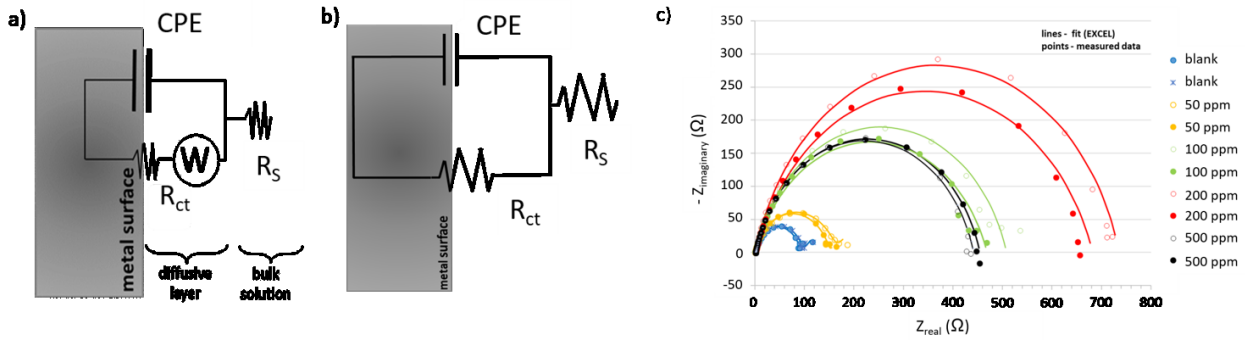

Figure 5: Equivalent electric circuits used for modelling of the EIS data: a) Randles cell including Warburg impedance in parallel to the CPE valid for 0 – 50 ppm inhibitor concentration. b) Simple Randles cell for inhibitor concentrations ≥ 100 ppm. c) Nyquist plot for uninhibited and inhibited brine.

Table 6: Best fit data of EIS measurements.

c	*OCP*	R_s	R_{ct}	*CPE*		*W*	*IE*	*SND**
(ppm)	(mV)	(Ω)	(Ω)	Q (µF)	n(-)	(DW)	(%)	(-)
0	-668	2.25	93	272	0.85	7.5	0	0.01
50	-643	0.74	152	244	0.85	-	38	0.05
100	-627	0.97	507	92	0.82	-	82	0.09
200	-630	1.21	734	67	0.84	-	87	0.07
500	-634	1.28	453	112	0.83	-	79	0.04

The obtained results show that the performance of the inhibitor is a complex interplay between atmosphere, brine composition and the chemical structure of the inhibitor. To sum up the observed performance of the inhibitor the following inhibition mechanisms in the present geothermal environment are assumed: (1) The adsorption on the metal surface mainly occurs through the adsorption of nitrogen by sharing its two free valence electrons with positively charged compounds on the metal. The hydrophobic tail is oriented towards the electrolyte solution and hinders water molecules to adsorb. (2) In the O_2-bearing environment, a competitive behavior between the nitrogen compounds and oxygen molecules is observed. (3) In addition, competitive behavior is also observed with chloride ions. (4) Moreover, the inhibitor may adsorb on free iron particles. (5) In case of CO_2-saturation, a co-operative adsorption between the inhibitor and a porous carbonate layer of iron and calcium oxides reduces the corrosion rate of the steel in the tested brine. (6) Further, in the original brine the interplay with organic films may influence the corrosion behavior.

4. CONCLUSION AND OUTLOOK

In this study, the inhibition effect of an imidazoline based corrosion inhibitor under geothermal conditions was characterized by means of different electrochemical and analytical measurement techniques (weight loss tests, potentiodynamic polarization scans, and electrochemical impedance spectroscopy). The inhibitor concentration, brine composition, exposure time and gas composition were varied. The test temperature was set up to 80°C representing the temperature found at the reinjection site of Soultz-sous-Forêts. The results display the complex interplay between brine, inhibitor and steel surface.

Depending on the operating conditions, one optimal inhibitor concentration could be identified. For weight loss and impedance measurements best inhibitor concentration was determined to be 200 ppm, whereas 100 ppm turned out to be the optimal concentration in the potentiodynamic polarization scans. The imidazoline inhibitor works much better in CO_2 than in O_2 saturated brines. A competitive adsorption behavior was identified for the inhibitor molecules and Cl-ions. The variation of the geothermal brine has a major influence on the inhibition efficiency. High saline brines and the presence of Ca^{2+} led to reduced inhibition efficiency compared to NaCl brine. None of the artificial brines matched the polarization behavior of the original brine sampled in the geothermal power plant in Soultz-sous-Forêts. The corrosion rate turned out to be significantly lower in the original brine, even without inhibition. This could be explained by the formation of scalings and passivation layers in the original brine. Therefore, detailed examination of the scalings and their mutual interaction with the inhibitor molecules is suggested for future research activities.

ACKNOWLEDGEMENT

This study was supported by the Program Oriented Funding of the Helmholtz Association of German Research Centers in the Program "Renewable Energies" in the Topic" Geothermal Energy Systems" (Project number 35.14.01)

REFERENCES

ASTM, Standard Practice for Standard Reference Method for Making Potentiostatic and Potentiodynamic Anodic Polarization Measurements, ASTM G5-82, ASTM International, (1985)

ASTM, Standard Practice for Preparing, Cleaning and Evaluating Corrosion Specimens, ASTM G1-03, ASTM International, (2011)

ASTM, Standard Practice for Calculation of Corrosion Rates and Related Information From Electrochemical Measurements, ASTM G102-89, ASTM International, (2010)

Baillieux, P., Schill, E., Edel J. and Mauri, G.: Localization of Temperature Anomalies in the Upper Rhine Graben: Insights from Geophysics and Neotectonic Activity, *International Geology Review* **55**, (2013), 1744-1762

Finsgar, M. and Jackson J.: Application of Corrosion Inhibitors for Steels in Acidic Media for the Oil and Gas Industry: A Review, *Corrosion Science* **86**, (2014), 17-41

Hernandez, J., Munoz, A., Genesca, J.: Formation of Iron-Carbonate Scale-Layer and Corrosion Mechanism of API X 770 Pipeline Steel in Carbon Dioxide-Saturated 3% Sodium Chloride, *Afinidad* **69**, (2012)

Heuer, J.K. and Stubbins, J.F.: An XPS Characterization of $FeCO_3$ films from CO_2 Corrosion, *Corrosion Science* **41**, (1999), 1231-1243

Heydari M. and Javidi M.: Corrosion inhibition and adsorption behaviour of an amido-imidazoline derivative on API 5L X52 steel in CO2-saturated solution and synergistic effect of iodide ions. *Corrosion Science* **61**, (2012), 148-155

Huttenloch, P., Zorn, R., Makni, L., Steger, H., Schilling, F., Hater, W.: Inhibitor Performance on Carbon Steel in the Geothermal Environment of the Upper Rhine Graben (Central Europe) – A Laboratory Study, *Geothermics* **81**, (2019), 198-208

Jevremović, I., Singer, M., Nešić, S., Mišković-Stanković, V.: Electrochemistry of carbon dioxide corrosion mitigation using tall oil diethylenetriamine imidazoline as corrosion inhibitor for mild steel, *Materials and Corrosion* **67**, (2016), 756-768

Jovancicevic, V., Ramachandran, S., Prince, P.: Inhibition of Carbon Dioxide Corrosion of Mild Steel by Imidazolines and Their Precursors, *Corrosion Science* **55**, (1999), 449-455

Lopez, D.A., Simison, S.N., De Sanchez, S.R.: The Influence of Steel Microstructure on CO_2 Corrosion. EIS Studies on the Inhibition Efficiency of Benzimidazole, *Electrochim. Acta* **48** (2003), 845‑854

Lui, D., Qui, Y.B., Tomoe, Y., Bando, K., Guo, X.P. : Interaction of Inhibitors with Corrosion Scale Formed on N80 Steel in CO_2-Saturated NaCl Solution, *Materials and Corrosion* **62**, (2011), 1153-1158

Liu, X. and Zheng, G.: Effect of Hydrophilic Group on Inhibition Behavior of Imidazoline for CO_2-Corrosion of N80 in 3%NaCl Solution, *Corrosion Engineering, Science and Technology* **43**, (2008), 87-92

Moreland, P.J. and Rowlands, C.: Methode und Instrumentierung bei Polarisationswiderstandsmessungen, *Materials and Corrosion* **28**, (1977), 249-258

Mundhenk, N., Huttenloch, P., Sanjuan, B., Kohl, T., Steger, H., Zorn, R.: Corrosion and Scaling as Interrelated Phenomena in an Operating Geothermal Power Plant, *Corrosion Science* **70**, (2013), 17-28

Nesic, S., Postlethwaite, J., Olsen, S.: An Electrochemical Model for Prediction of Corrosion of Mild Steel in Aqueous Carbon Dioxide Solutions, *Corrosion* **52**, (1996), 280-294

Ortega-Toledo, D.M., Gonzalez-Rodriguez, J.G., Casales, M., Neri-Florez, M.A., Martinez-Villafane, A.: The CO_2 corrosion inhibition of a high strength pipeline steel by hydroxyethyl imidazoline, *Materials Chemistry and Physics* **122**, (2010), 485-490

Pribnow, D. and Schellschmidt, R.: Thermal Tracking of Upper Crustal Fluid Flow in the Rhine Graben, *Geophysical Research Letters* **27**, (2000), 1957-1960

Sanjuan, B., Millot, R., Innocent, Ch., Dezayes, Ch., Scheiber, J., Brach, M.: Major Geochemical Characteristics of Geothermal Brines From the Upper Rhine Graben Granitic Basement with Constraints on Temperature and Circulation, *Chemical Geology* **428**, (2016), 27-47

Scheiber, J., Seibt, A., Birner, J., Genter, A., Cuenot, N., Moeckes, W.: Scale Inhibition at the Soultz-sous-Forets (France) EGS Site: Laboratory and On-site Studies, *Proceedings*, World Geothermal Congress, Melbourne Australia, (2015)

Tao, Z., Zhang, S., Li, W., Hou, B.: Corrosion Inhibition of Mild Steel in Acidic Solution by Some Oxo-Triazole Derivatives, *Corrosion Science* **51**, (2009), 2588-2595

Wu, S.L., Cui, Z.D., He, F., Bai, Z.Q., Yang, X.J.: Characterization of the Surface Film Formed from Carbon Dioxide Corrosion on N80 Steel, *Materials Letters* **58**, (2004), 1076-1081

Zhang, G., Chen, C., Lu, M., Chai, C., Wu, Y.: Evaluation of Inhibition Efficiency of an Imidazoline Derivative in CO_2-Containing Aqueous Solution, *Materials Chemistry and Physics* **105**, (2007), 331-340